Progress In Electromagnetics Research M, Vol. 93, 1–9, 2020

A Polarization Reconfigurable Cylindrical Dielectric Resonator Antenna

Lei Zhong*

Abstract—A reconfigurable cylindrical dielectric resonator antenna with polarization diversity is proposed for S-band and C-band in this paper. An annular slot is used as the feeding aperture, which can not only excite two orthogonal modes ($HEM^x_{11\delta}$ and $HEM^y_{11\delta}$) of the cylindrical dielectric resonator at 3.2 GHz, but also produce a 90° phase difference. Two switches, whose locations are carefully optimized, are used to control $HEM^x_{11\delta}$ being a phase-lagging or phase-leading component. Thus the antenna can achieve either left- or right-hand circular polarization (LHCP or RHCP) in S band, depending on the switch states. The higher order mode of $HEM_{21\delta}$ is also excited at 4.7 GHz for linear polarization (LP), regardless of the switch states. With the advantages of compact structure, simple biasing network and easy fabrication, this antenna can be widely applied to wireless communication systems, especially for polarization diversity applications.

1. INTRODUCTION

Dielectric resonator antennas (DRAs) have been widely researched since 1983 [1], for their attractive advantages of low loss, compact size and simple feeding mechanism. By choosing different dielectric resonator (DR) shapes and feeding structures, various modes of DR can be obtained for different radiation patterns, which makes the DRA a good candidate for diversity or multi-function systems.

Recently, circularly polarized (CP) DRAs and dual-band DRAs have received tremendous attention. Because the dual-band DRA can reduce the size, mass, complexity and cost significantly, and CP is suitable for addressing challenges from mobility, adverse weather conditions and no-line-of sight applications. To design dual-band DRAs, one can use a second DR [2], a fractal-shaped DR [3, 4], a parasitic slot [5], or a high-order mode [6, 7]. While the reported CP DRAs can be classified into: (a) novel DR geometry form, including slotted DRA [8], rotated stacked DRA [9, 10] and strip loaded DRA [11], and (b) multiple feed regular-shaped DRA form, such as aperture-fed DRA [12], differential-fed [13], quadrature-fed DRA [14] and spiral-slot-fed DRA [15].

However, most CP DRAs mentioned above can only transmit and receive either RHCP or LHCP. It is necessary to study the CP DRA with polarization diversity to avoid the polarization mismatch and to improve the link quality. Polarization diversity can be achieved by polarization reconfigurable antenna (PRA), which can dynamically alter its polarizations by changing the field distribution in the antenna with switches [16].

In this paper, a reconfigurable cylindrical dielectric resonator antenna (CDRA) with polarization diversity is proposed for S and C bands. An annular slot is used to excite three modes of CDR, including two equal-amplitude and orthogonal modes ($HEM^x_{11\delta}$ and $HEM^y_{11\delta}$) at 3.2 GHz, and a $HEM_{21\delta}$ at 4.7 GHz. With properly controlling of PIN diodes, the CDRA can generate an LHCP or RHCP wave in S band. For each CP sense, the antenna exhibits wide impedance and 3 dB axial ratio bandwidths and stable radiation patterns, while the CDRA remains LP in the C band when the diode states are switched, because the $HEM_{21\delta}$ mode is symmetrical. Simulation and measurement results show good agreement.

Received 8 April 2020, Accepted 6 May 2020, Scheduled 17 May 2020
* Corresponding author: Lei Zhong (albertzhonglei@163.com).
The author is with the Southwest China Research Institute of Electronic Equipment, Chengdu, China.

2. ANTENNA DESIGN

The schematic of the proposed reconfigurable CDRA is shown in Fig. 1, in which a CDR is centered above a grounded square Rogers RO4003C substrate (thickness $h_s = 0.5\,\text{mm}$, permittivity $\varepsilon_{rs} = 3.38$, loss tangent $\tan\delta = 0.0027$). The CDR has a dielectric constant of $\varepsilon_{rd} = 10$, and a radius of a and a height of h. If the ratio of radius and height satisfies $0.4 < a/h < 6$, the resonant frequency of $\text{HEM}_{11\delta}$ mode can be calculated by the following analytic formula [17, 18]

$$f_{11\delta} = \frac{c}{2\pi a}\frac{6.324}{\sqrt{\varepsilon_{rd}+2}}\left[0.27 + 0.36\left(\frac{a}{2h}\right) + 0.02\left(\frac{a}{2h}\right)^2\right] \tag{1}$$

where c is the velocity of light in free space.

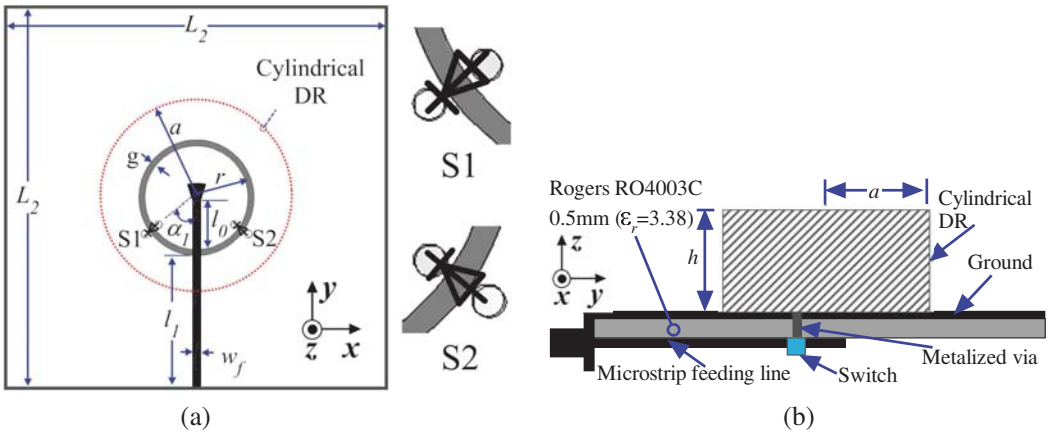

Figure 1. Geometry of the proposed DRA. (a) Top view, (b) side view. (Parameters are the following: $a = 12\,\text{mm}$, $h = 13\,\text{mm}$, $r = 6.8\,\text{mm}$, $g = 0.8\,\text{mm}$, $w_f = 1.1\,\text{mm}$, $\alpha_1 = 55.2°$, $l_0 = 6.4\,\text{mm}$, $l_1 = 17.4\,\text{mm}$, $L_2 = 50\,\text{mm}$.).

The proposed DRA is excited by a $50\,\Omega$ microstrip feeding line through an annular slot etched in the ground, shown in Fig. 1(a). A microstrip radial stub is connected to the end of microstrip line for impedance matching [19], whose flare angle is 60° and radius is 3.6 mm.

The annular slot is utilized as the coupling aperture, because it is symmetrical and rotation invariant. Rotation invariance provides the possibility to excite two orthogonal modes at the same time. The symmetry on the y axis makes it easy to achieve reconfigurable circular polarizations. Since a 90° phase difference is necessary for CP radiation, the quarter of annular slot circumference should equal to a quarter wavelength of $f_{11\delta}$. Therefore, the radius r of the annular slot should be

$$r = \frac{c}{2\pi f_{11\delta}\sqrt{\varepsilon_{rs}}}. \tag{2}$$

As shown in Fig. 1(a), two switches (S1 and S2) are placed symmetrically about the feeding line to create short circuits in the annular slot, thus a 90° or −90° phase difference between two orthogonal modes is achieved for LHCP or RHCP. The angle (α_1) between S1 and the feeding line is carefully optimized for impedance matching.

Two BAR64-02V PIN diodes from Infineon Technologies are used as the switches [16]. According to the data sheet, the PIN diode at ON and OFF states can be equivalent to an ohmic resistance of ($R_f = 2.1\,\Omega$) and a parallel RC circuit with the resistance of ($R_p = 3000\,\Omega$) and the capacitance of ($C_p = 0.17\,\text{pF}$), respectively. The equivalent circuit of diode is shown in Fig. 2. Since the DC bias voltage is 3 V, a $47\,\Omega$ current limiting resistor is added. Two RF choke inductors (100 nH) are used as the bias network for diodes. To minimize influence of switches on antenna performance, the CDR and switches are located on different sides of the substrate, shown in Fig. 1(b). Two pairs of metallized vias are operated to connect switches to the ground.

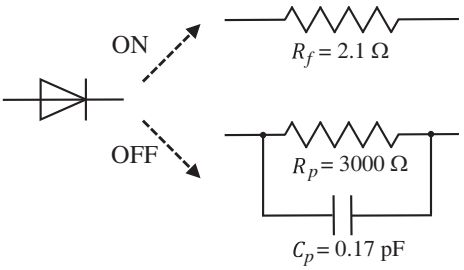

Figure 2. Equivalent circuit of BAR64-02V PIN diode at ON and OFF states.

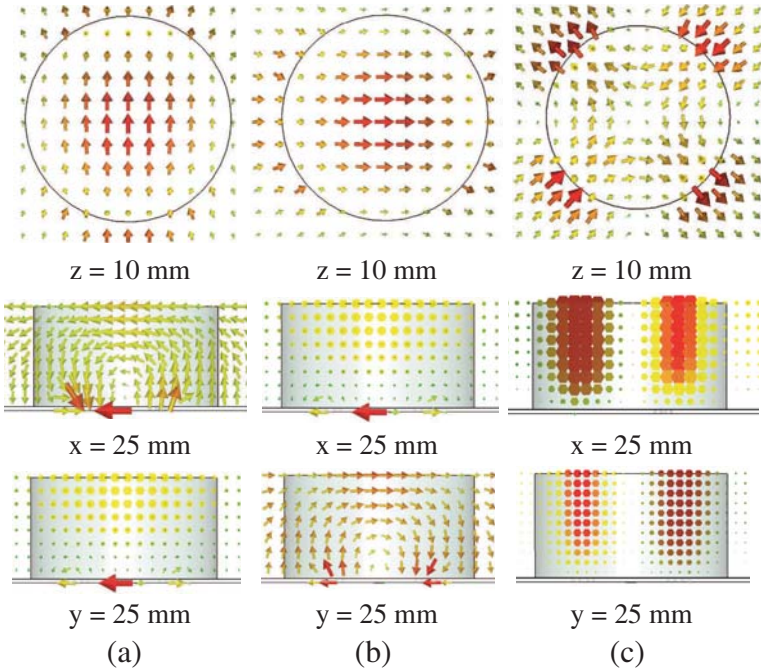

Figure 3. Electric field distributions of the excited modes in the CDRA. (a) $\mathrm{HEM}^{x}_{11\delta}$, (b) $\mathrm{HEM}^{y}_{11\delta}$, (c) $\mathrm{HEM}_{21\delta}$.

Figure 3 shows the electric field distributions of three excited modes, which are obtained by an eigenmode analysis (without excitation and switches). The results show that the CDR could resonant in $\mathrm{HEM}^{x}_{11\delta}$, $\mathrm{HEM}^{y}_{11\delta}$ and $\mathrm{HEM}_{21\delta}$ modes at 3.3472 GHz, 3.4253 GHz and 4.5889 GHz respectively.

Polarization control way is summarized in Table 1. The simulated electric field distributions at 3.2 GHz and 4.7 GHz are plotted in Fig. 4. The antenna radiates an RHCP wave at S-band, when the switch S1 is ON and S2 is OFF. Conversely, LHCP will be obtained in $\mathrm{M2_{LH}}$ mode, while an LP wave is realized at C-band for both modes, because the $\mathrm{HEM}_{21\delta}$ mode is symmetrical, and the switch states almost do not affect the field distributions.

Table 1. Polarization sense control via two switches.

Mode	Switch States		Polarization	
	S_1	S_2	S-band	C-band
$\mathrm{M1_{RH}}$	ON	OFF	RHCP	LP
$\mathrm{M2_{LH}}$	OFF	ON	LHCP	LP

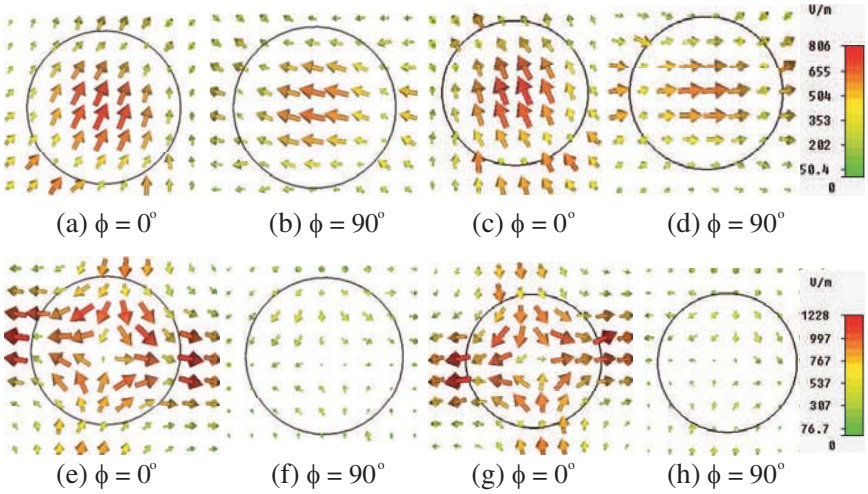

Figure 4. Simulated electric field distributions in top views ($z = 10\,\text{mm}$) for (a) (b) M1_{RH} at 3.2 GHz, (c) (d) M2_{LH} at 3.2 GHz, (e) (f) M1_{RH} at 4.7 GHz, (g) (h) M2_{LH} at 4.7 GHz.

3. RESULTS AND ANALYSIS

As the antenna has a symmetrical structure, M1_{RH} mode is taken as an example for parametric studies, which are performed by CST Microwave Studio. Fig. 5 illustrates the simulated reflection coefficients ($|S_{11}|$) and the axial ratios (AR) for different CDR radii. It is found that both the impedance and AR bands shift downward with an increase of CDR's radius, which is expected because a larger DR should have a lower resonance frequency.

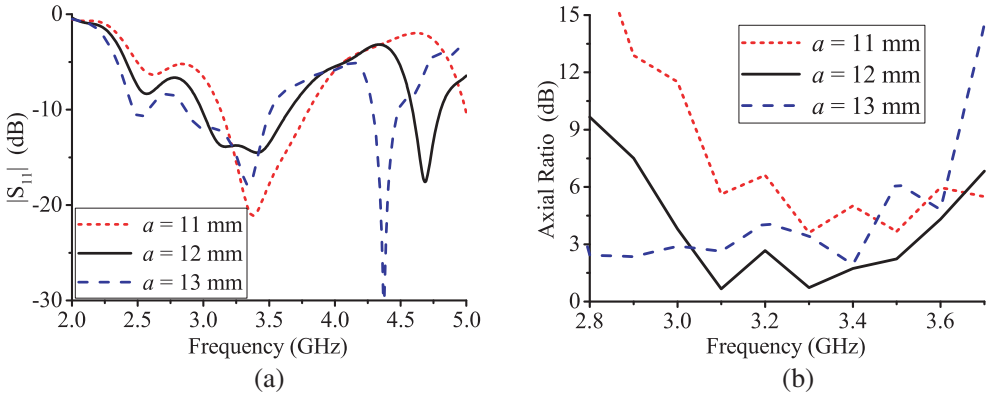

Figure 5. Simulated $|S_{11}|$ and AR for different CDR radii. (a) $|S_{11}|$, (b) AR.

The influence of the annular slot radius r on matching and CP is studied in Fig. 6. If the radius r increases from 6.6 mm to 8.6 mm, the -10 dB impedance bandwidth decreases from 32.4% to 20.9%, while the AR values decrease first and then increase. Because AR depends on both magnitudes and phase difference between $\text{HEM}^{x}_{11\delta}$ and $\text{HEM}^{y}_{11\delta}$. According to Equation (2), a quarter circumference of annular slot should provide a 90° phase difference for CP at 3.2 GHz. When the circumference increases with r, the phase difference will be increased from less than 90° to more than 90°. The changes in Fig. 6(b) verify our design method. Fig. 7 shows the effect of switch location α_1. When the α_1 varies, the changes in $|S_{11}|$ and AR are relatively mild thus, α_1 can be used for fine-tuning.

As a simple design guideline, one can choose the DR's size according to the operating frequency, can use annular slot size to optimize the AR, and can fine tune the antenna by setting other parameters, such as α_1, g and l_0.

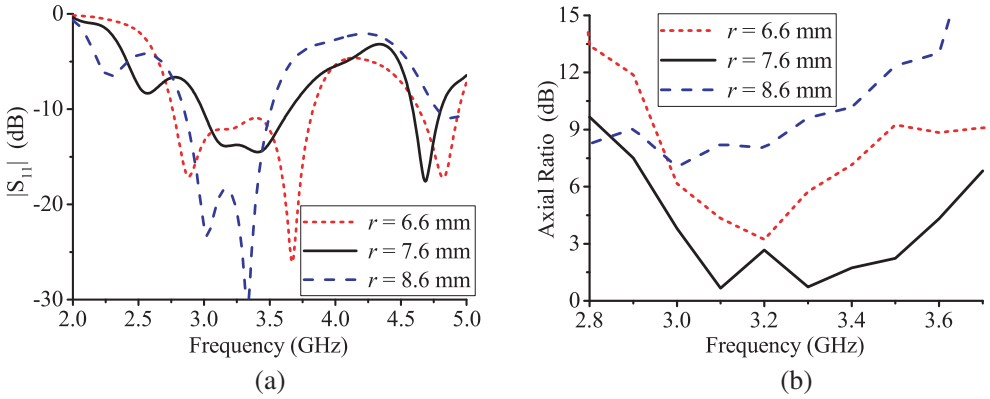

Figure 6. Simulated $|S_{11}|$ and AR for different values of r. (a) $|S_{11}|$, (b) AR.

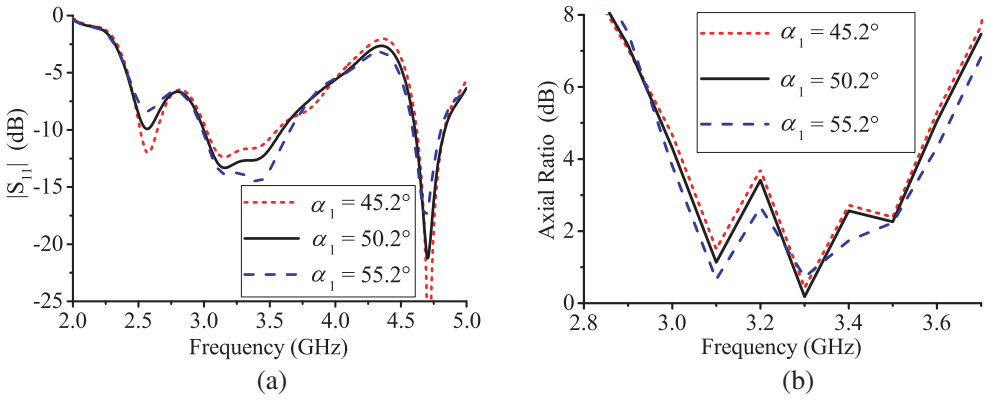

Figure 7. Simulated $|S_{11}|$ and AR for different values of α_1. (a) $|S_{11}|$, (b) AR.

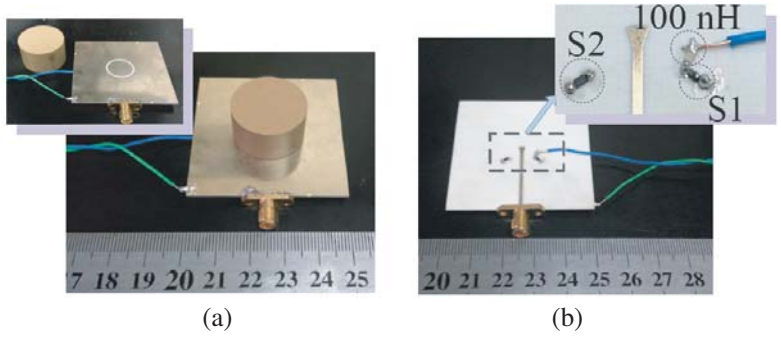

Figure 8. Fabricated reconfigurable cylindrical DRA prototype. (a) Front view, (b) back view. DRA: $\varepsilon_{rd} = 10$, $D = 24\,\text{mm}$, $h = 13\,\text{mm}$.

To verify the proposed design, a prototype antenna is fabricated and measured, shown as in Fig. 8. The CDR is cut from a thick dielectric block by a CNC machine tool, while the grounded Rogers RO4003C substrate is processed by PCB technology. The DC bias circuit and PIN diodes are manually welded on the substrate. The S-parameters and radiation characteristics are measured by the ZVB20 vector network analyzer from Rohde & Schwarz and the StarLab antenna measurement system from SATIMO, respectively.

Figure 9 shows the simulated and measured S-parameters (dB) results of two modes. The measured $-10\,\text{dB}$ bandwidths of M1_{RH} are about 3.12–3.61 GHz (490 MHz, 14.56%) and 4.6–4.76 GHz (160 MHz,

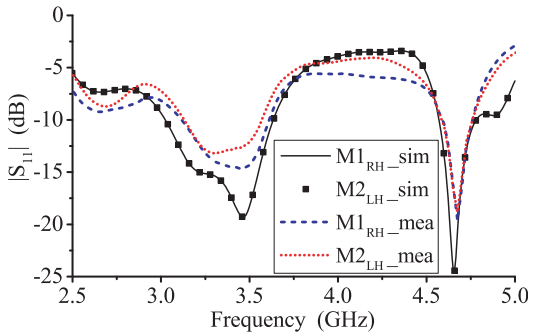

Figure 9. .Simulated and measured reflection coefficients $|S_{11}|$.

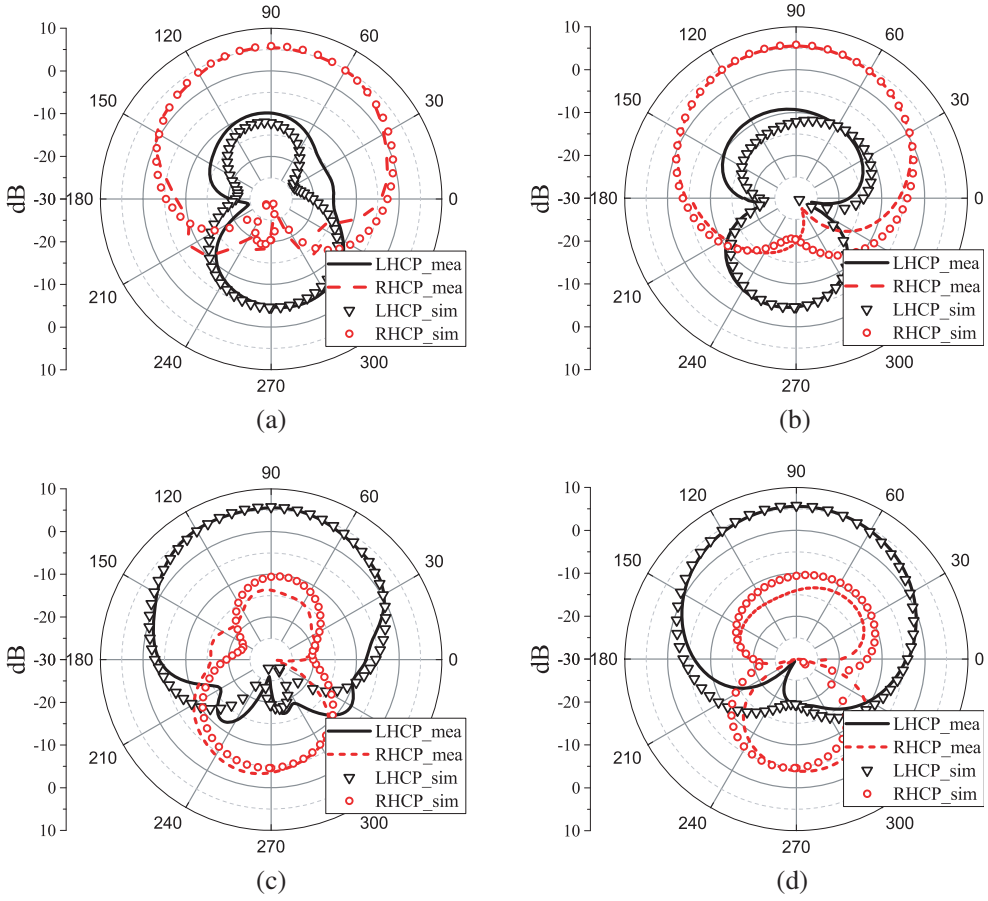

Figure 10. Simulated and measured radiation patterns at 3.2 GHz. (a) *xoz*-plane for $M1_{RH}$, (b) *yoz*-plane for $M1_{RH}$, (c) *xoz*-plane for $M2_{LH}$, (d) *yoz*-plane for $M2_{LH}$.

3.42%) for S-band and C-band, respectively, while those for $M2_{LH}$ are about 3.14–3.56 GHz (420 MHz, 12.54%) and 4.59–4.76 GHz (170 MHz, 3.64%). Generally, the measured results agree well with the simulated results, except for a narrower bandwidth. The difference may be caused by the bias network and assembly tolerances.

Figure 10 depicts the radiation patterns of $M1_{RH}$ and $M2_{LH}$ at S-band, respectively. For both modes, broadside radiation patterns are measured, which are very close with the simulation. The measured half power beam widths (HPBW) are about 90.5° along *xoz*-plane and 88.2° along *yoz*-plane. For $M1_{RH}$ mode, the RHCP fields are 15.3 dB stronger than LHCP in the boresight direction, while

the LHCP is about 18 dB stronger than RHCP in $M2_{LH}$. The measured results also confirm that the patterns of proposed antenna are symmetrical and quite stable when the polarization is switched.

The radiation patterns at C-band of $M1_{RH}$ and $M2_{LH}$ are shown in Fig. 11. The main lobe direction is about 45° away from the z-axis positive direction. Compared with patterns at S-band, the patterns in C-band split into two half beams in both xoz- and yoz-plane. Because the electric field distributions of $HEM_{21\delta}$ are symmetrical about both x and y axes, which also weaken the effect of switches in C-band.

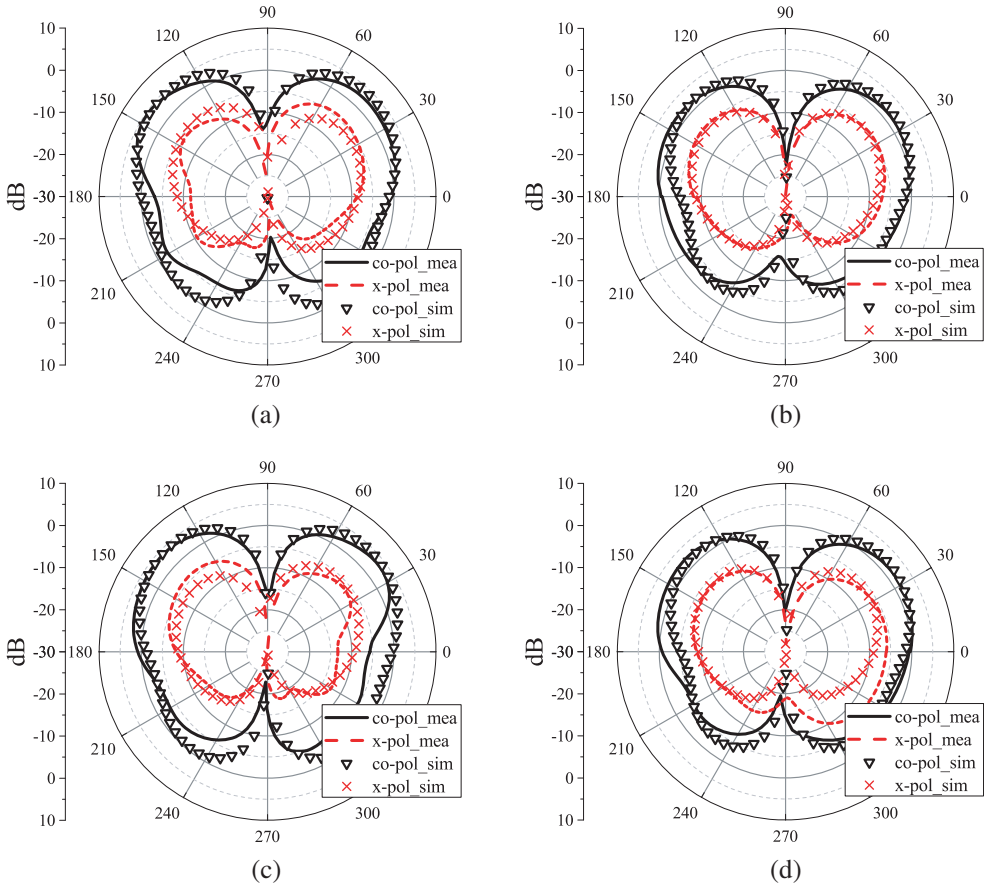

Figure 11. Simulated and measured radiation patterns at 4.7 GHz. (a) xoz-plane for $M1_{RH}$, (b) yoz-plane for $M1_{RH}$, (c) xoz-plane for $M2_{LH}$, (d) yoz-plane for $M2_{LH}$.

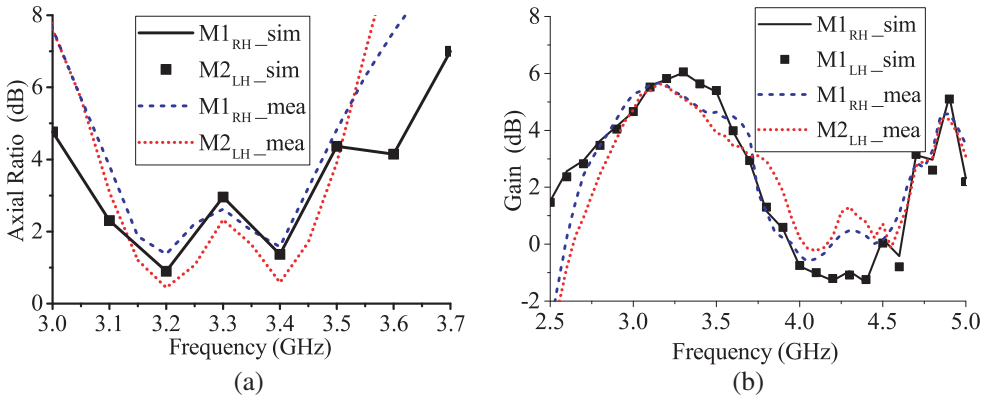

Figure 12. (a) Measured AR for $M1_{RH}$ and $M2_{LH}$, (b) measured gain.

The measured axial ratio curves, in the boresight direction, of two CP operations are plotted versus frequency in Fig. 12(a). The measured 3 dB AR bandwidths are about 3.14–3.42 GHz (280 MHz, 8.54%) and 3.13–3.45 GHz (320 MHz, 9.73%) for $M1_{RH}$ and $M2_{LH}$, respectively. As illustrated in Fig. 12(b), the measured maximal gain values in S-band are 5.67 dB at 3.2 GHz and 5.65 dB at 3.22 GHz for $M1_{RH}$ and $M2_{LH}$. Those values of C-band are 4.58 dB and 4.42 dB.

4. CONCLUSION

A new circular-polarization-reconfigurable cylindrical dielectric resonator antenna operating at S-band is demonstrated in this work, which can also provide LP at C-band. For the first time, an annular slot is used to excite two equal-amplitude and orthogonal modes ($HEM^{x}_{11\delta}$ and $HEM^{y}_{11\delta}$) and to provide 90° phase difference at the same time. The antenna has advantages of compact structure, simple biasing network, easy fabrication and adjustment, which can be widely applied to wireless communication systems, especially for polarization diversity applications.

REFERENCES

1. Long, S., M. McAllister, and L. Shen, "The resonant cylindrical dielectric cavity antenna," *IEEE Trans. Antennas Propag.*, Vol. 31, No. 3, 406–412, 1983.
2. Fan, Z. and Y. Antar, "Slot-coupled dr antenna for dual-frequency operation," *IEEE Trans. Antennas Propag.*, Vol. 45, No. 2, 306–308, 1997.
3. Liu, H., Y. Liu, M. Wei, and S. Gong, "Dual-broadband dielectric resonator antenna based on modified sierpinski fractal geometry," *Electron. Lett.*, Vol. 51, No. 11, 806–808, 2015.
4. Altaf, A., J. Jung, Y. Yang, K. Lee, and K. C. Hwang, "Reconfigurable dual-/triple-band circularly polarized dielectric resonator antenna," *IEEE Antennas and Wireless Propagation Letters*, Vol. 19, No. 3, 443–447, 2020.
5. Chen, H.-M., Y.-K. Wang, Y.-F. Lin, S.-C. Lin, and S.-C. Pan, "A compact dual-band dielectric resonator antenna using a parasitic slot," *IEEE Antennas and Wireless Propagation Letters*, Vol. 8, 173–176, 2009.
6. Guha, D., P. Gupta, and C. Kumar, "Dualband cylindrical dielectric resonator antenna employing $HEM_{11\delta}$ and $HEM_{12\delta}$ modes excited by new composite aperture," *IEEE Trans. Antennas Propag.*, Vol. 63, No. 1, 433–438, 2015.
7. Sharma, A., G. Das, S. Gupta, and R. K. Gangwar, "Quad-band quad-sense circularly polarized dielectric resonator antenna for gps/cnss/wlan/wimax applications," *IEEE Antennas and Wireless Propagation Letters*, Vol. 19, No. 3, 403–407, 2020.
8. Fang, X., K. W. Leung, and E. H. Lim, "Singly-fed dual-band circularly polarized dielectric resonator antenna," *IEEE Antennas and Wireless Propagation Letters*, Vol. 13, 995–998, 2014.
9. Wang, K. X. and H. Wong, "A circularly polarized antenna by using rotated-stair dielectric resonator," *IEEE Antennas and Wireless Propagation Letters*, Vol. 14, 787–790, 2015.
10. Chowdhury, R. and R. K. Chaudhary, "An approach to generate circular polarization in a modified cylindrical-shaped dielectric resonator antenna using pmc boundary approximation," *IEEE Antennas and Wireless Propagation Letters*, Vol. 17, No. 9, 1727–1731, 2018.
11. Motevasselian, A., A. Ellgardt, and B. Jonsson, "A helix excited circularly polarized hollow cylindrical dielectric resonator antenna," *IEEE Antennas and Wireless Propagation Letters*, Vol. 12, 535–538, 2013.
12. Chair, R., S. S. Yang, A. Kishk, K. F. Lee, K. M. Luk, et al., "Aperture fed wideband circularly polarized rectangular stair shaped dielectric resonator antenna," *IEEE Trans. Antennas Propag.*, Vol. 54, No. 4, 1350–1352, 2006.
13. Wang, X., S. Tang, L. Yang, and J. Chen, "Differential-fed dual-polarized dielectric patch antenna with gain enhancement based on higher order modes," *IEEE Antennas and Wireless Propagation Letters*, Vol. 19, No. 3, 502–506, 2020.

14. Lim, E. H., K. W. Leung, and X. Fang, "The compact circularly-polarized hollow rectangular dielectric resonator antenna with an underlaid quadrature coupler," *IEEE Trans. Antennas Propag.*, Vol. 59, No. 1, 288–293, 2011.
15. Zou, M., J. Pan, and Z. Nie, "A wideband circularly polarized rectangular dielectric resonator antenna excited by an archimedean spiral slot," *IEEE Antennas and Wireless Propagation Letters*, Vol. 14, 446–449, 2015.
16. Zhong, L., J. S. Hong, and H. C. Zhou, "A novel pattern-reconfigurable cylindrical dielectric resonator antenna with enhanced gain," *IEEE Antennas and Wireless Propagation Letters*, Vol. 15, 1253–1256, 2016.
17. Guha, D., H. Gajera, and C. Kumar, "Cross-polarized radiation in a cylindrical dielectric resonator antenna: Identification of source, experimental proof, and its suppression," *IEEE Trans. Antennas Propag.*, Vol. 63, No. 4, 1863–1867, 2015.
18. Luk, K. M. and K. W. Leung, *Dielectric Resonator Antennas*, Research Studies Press, Hertfordshire, U.K., 2003.
19. Garg, R., I. Bahl, and M. Bozzi, *Microstrip Lines and Slotlines*, Artech House, 2013.